nature climate change

LETTERS

PUBLISHED ONLINE: 10 APRIL 2017 | DOI: 10.1038/NCLIMATE3263

Human-induced erosion has offset one-third of carbon emissions from land cover change

Zhengang Wang[1]*, Thomas Hoffmann[2,3], Johan Six[4], Jed O. Kaplan[5], Gerard Govers[6], Sebastian Doetterl[7,8] and Kristof Van Oost[1]

Anthropogenic land cover change (ALCC) is an important carbon (C) loss mechanism[1–3], but current methods do not consider the role of accelerated soil organic C erosion and its burial in sediments in their assessments of net soil–atmosphere C exchange. Using a comprehensive global database and parsimonious modelling, we evaluate the impact of anthropogenic soil erosion on C fluxes between the Earth's surface and atmosphere from the onset of agriculture to the present day. We find that agricultural erosion represents a very large and transient perturbation to the C cycle and has induced a cumulative net uptake of 78 ± 22 Pg C in terrestrial ecosystems during the period 6000 BC to AD 2015. This erosion-induced soil organic C sink is estimated to have offset 37 ± 10% of previously recognized C emissions resulting from ALCC. We estimate that rates of C burial have increased by a factor of 4.6 since AD 1850. Thus, current assessments may significantly overestimate both past and future anthropogenic emissions from the land. Given that ALCC is the most uncertain component of the global C budget and that there is a strong connection between ALCC and erosion, an explicit representation of erosion and burial processes is essential to fully understand the impact of human activities on the net soil–atmosphere C exchange.

Erosion of active orogens, at geologic timescales, has long been recognized to regulate atmospheric CO_2 and climate through silicate weathering[4,5] and organic C burial in sediments[6–8]. However, the role of human-induced erosion and burial of soil organic carbon (SOC) is usually omitted from climate studies that focus on decadal to centennial timescales. This is a significant source of bias given that human activity is currently considered to be the dominant force driving erosion and burial, with the conversion of natural land cover to cropland accelerating erosion and burial by one to two orders of magnitude[9,10].

Since the start of agriculture several thousand years ago, humans have drastically altered the global C cycle by transforming vast areas with natural vegetation to human use, primarily by the expansion of agriculture. Emissions from ALCC are one of the largest anthropogenic sources of atmospheric CO_2 and are the most uncertain component of both the past[2,11] and present[1] global C cycle. Although current coupled C cycle–climate models do represent the impact that humans have had on CO_2 uptake and release by plants and on the decomposition of organic C stored in litter and soils, they do not account for the substantial acceleration of erosion and burial that accompanies ALCC. Nevertheless, there is growing recognition that the human-induced acceleration of erosion, transport and burial of C has a significant impact on the global C cycle[12,13].

As schematically represented in Fig. 1, erosion processes operate across various spatial scales that characterize the geomorphic cascade. Along this cascade, C originally fixed by land plants is continuously displaced laterally along the Earth's surface, from upland soils to streams and rivers and eventually oceans. Here, we examined the effect of erosion on the terrestrial C budget from the onset of agriculture (6000 BC) to the present day using evidence from: a global synthesis of ALCC and accelerated erosion spanning the entire period of agriculture; a global analysis of changes in SOC along the geomorphic cascade from sedimentary sources to sinks; and a coupled erosion–C cycling model (see Methods). In our analysis, we considered the following compartments of the geomorphic cascade: stable soils not affected by erosion, eroding slopes in upland areas, depositional storage in uplands (colluvial deposition), storage of overbank sediments in both cropland and non-cropland floodplains (alluvial deposition), transport of sediments in rivers, and storage in lakes, man-made reservoirs and, finally, ocean sediments.

To reconstruct long-term fluxes of sediment across the Earth's surface we used an erosion–deposition model based on land use, climate and relief[14]. The model was trained and evaluated on a database of 13 catchments covering a large variety of agricultural trajectories (varying in duration between 150 and 7,000 years) and environmental conditions (Supplementary Table 1). Our model predictions show no systematic bias and provide sediment flux predictions with relative errors of about 25% (Fig. 2). These findings, and their consistency with independently derived estimates, give confidence that the model can be used to give realistic estimates of the erosional disturbance following agricultural land conversion across the globe.

To assess the effects of erosion and deposition on local SOC storage, we carried out a global and comprehensive analysis of 6,580 soil profiles and extracted information on the geomorphic position of these profiles from either topographical attributes or soil profile descriptions (see Methods). These SOC profiles represent a wide range of climatic conditions and span the spectrum of geomorphic contexts found in agricultural landscapes across the globe (Fig. 3). Because the model used to describe the SOC profiles (equation (1) in Methods) does not account for variability in lithology, vegetation characteristics and land use history and management, the model is not a good estimator everywhere. However, in almost all cases, modelled SOC profiles for each

[1]Georges Lemaître Center for Earth and Climate Research (TECLIM), Earth and Life Institute, Université catholique de Louvain, 1348 Louvain-la-Neuve, Belgium. [2]Department of Geography, University of Bonn, Meckenheimer Allee 166, 53115 Bonn, Germany. [3]German Federal Institute of Hydrology, Am Mainzer Tor 1, 56068 Koblenz, Germany. [4]Department of Environmental Systems Science, Swiss Federal Institute of Technology, ETH Zurich, 8092 Zurich, Switzerland. [5]Institute of Earth Surface Dynamics, University of Lausanne, Geopolis, 1015 Lausanne, Switzerland. [6]Department of Earth and Environmental Sciences, K.U. Leuven, 3001 Heverlee, Belgium. [7]Institute of Geography, Augsburg University, Alter Postweg 118, 86159 Augsburg, Germany. [8]ISOFYS-Isotope Bioscience Laboratory, Ghent University, Coupure Links 653, 9000 Gent, Belgium. *e-mail: zhengang.wang@uclouvain.be

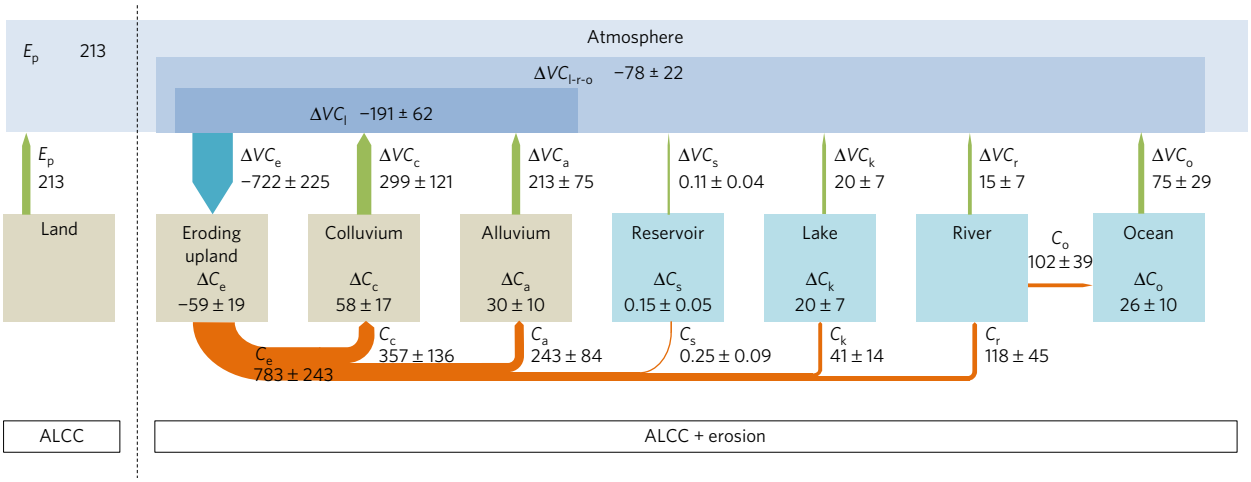

Figure 1 | Component fluxes of the erosion-induced C budget for the period of agriculture. The arrows represent the cumulative lateral and vertical (that is, land–atmosphere) C fluxes induced by agricultural soil erosion (Pg C). Traditional approaches considered only the primary emission from ALCC (E_p), that is, the C release due to a reduction in vegetation and soil C. Here we present a full source-to-sink analysis across the geomorphic cascade: C_e, C_c, C_a, C_s, C_k, C_r and C_o denote SOC mobilization by erosion, SOC burial in colluvial and alluvial stores, SOC buried in reservoirs and lakes, and SOC export to the river and ocean, respectively, while ΔC_e, ΔC_c, ΔC_a, ΔC_s, ΔC_k and ΔC_o represent the C stock variation of the eroding, colluvial deposition and alluvial deposition areas and the preserved terrestrial POC in the reservoirs, lakes and oceans, respectively. Positive C stock variation values indicate SOC sequestration while negative values indicate SOC loss. The erosion-induced vertical soil–atmosphere fluxes are represented by ΔVC_e, ΔVC_c and ΔVC_a to denote the vertical C fluxes of eroding uplands, colluvial and alluvial deposition areas, respectively; ΔVC_s, ΔVC_k, ΔVC_r and ΔVC_o denote the erosion-induced vertical C flux of the reservoirs, lakes, rivers and oceans, respectively; ΔVC_l and $\Delta VC_{l\text{-}r\text{-}o}$ denote the net erosion-induced vertical C flux of the land and land–river–ocean system, respectively. Negative values denote a flux towards the land; positive values denote a flux towards the atmosphere. The median value of the simulation is presented as the best prediction, while errors represent the 25th and 75th percentile ranges.

geomorphic–climate class combination were significantly different from their non-eroding counterparts (Fig. 3), and the model provides robust estimates of average SOC depth profiles along the geomorphic cascade (Supplementary Fig. 4).

Assuming that our estimate of past erosion is realistic and that the global SOC profile analysis describes well the changes in SOC under the impact of erosion processes (see Methods), we ran our model at the global scale for the period of agriculture (6000 BC–AD 2015). The model tracks the transfer and/or burial of sediment and associated SOC from sources to sinks. Estimates of changes in SOC stocks were then combined with the simulated lateral SOC fluxes to infer erosion-induced soil–atmosphere C exchange[15]. Mineralization and C burial in aquatic environments were constrained by data from the literature (see Supplementary Methods 3 Section 4.3). By considering 10,000 scenarios, we explicitly accounted for uncertainty in both model inputs and parameters.

We obtained a global cumulative agricultural sediment flux of 31,000 ± 9,000 Pg for the agricultural period. This erosional disturbance resulted in large lateral fluxes and transfer of SOC along the sediment cascade. Accounting for uncertainties in SOC stock, erosion rates and C enrichment ratios, we estimated a cumulative SOC mobilization (C_e) of 783 ± 243 Pg (Fig. 1), of which about 92% was mobilized during the pre-industrial period (that is, before AD 1850). At eroding sites, two competing processes operate: an erosion-induced decline in net primary production (NPP) reduces soil C inputs[16] while the stabilization of fresh C inputs into newly exposed subsoil enhances C uptake[17,18]. Soil erosion reduces soil depth and modifies soil properties, which may have a detrimental effect on NPP through the decrease of the supply of water, nutrients and rooting space[19]. At the same time, C-depleted subsoil material is brought to the surface layers where it can be mixed with fresh photosynthetically derived C inputs. This additional C uptake may (at least partially) replace the laterally lost SOC due to erosion[18,20]. Despite a lateral loss of 783 ± 243 Pg SOC, a comparison of SOC profiles between stable and eroding areas showed that SOC stocks in eroding uplands decreased by only 59 ± 19 Pg over the

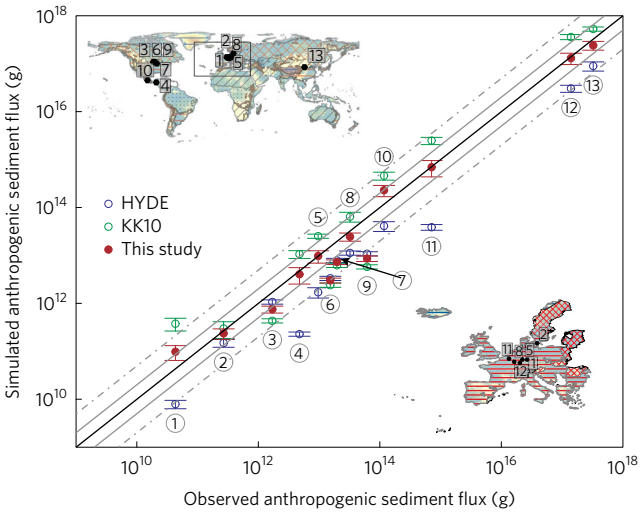

Figure 2 | Comparison of observed and simulated cumulative anthropogenic sediment fluxes. The numbers in circles denote the identification of the catchment, which is shown in Supplementary Table 1. Observed fluxes are estimates of the total anthropogenic sediment flux in the catchment over the agricultural period. HYDE and KK10 denote the predictions using the HYDE and KK10 land use scenarios. The filled red dots show the predictions made using this study's land use scenario that combines both HYDE and KK10. The error bars show the interquartile range (25% to 75%) of the distributions (obtained from Monte Carlo scenarios) associated with each prediction. The black solid line denotes the ratio of 1:1. The grey solid lines denote 1:2 and 2:1 ratios. The grey dashed lines denote 1:5 and 5:1 ratios. The insets show the locations of these catchments, with the background colour indicating elevation and hatching indicating the climatic zone (dots: tropical; slashed lines: dry; red horizontal lines: temperate; crossed lines: continental; blue horizontal lines: polar). The inset in the lower right corner represents the region in the rectangle in the upper left corner.

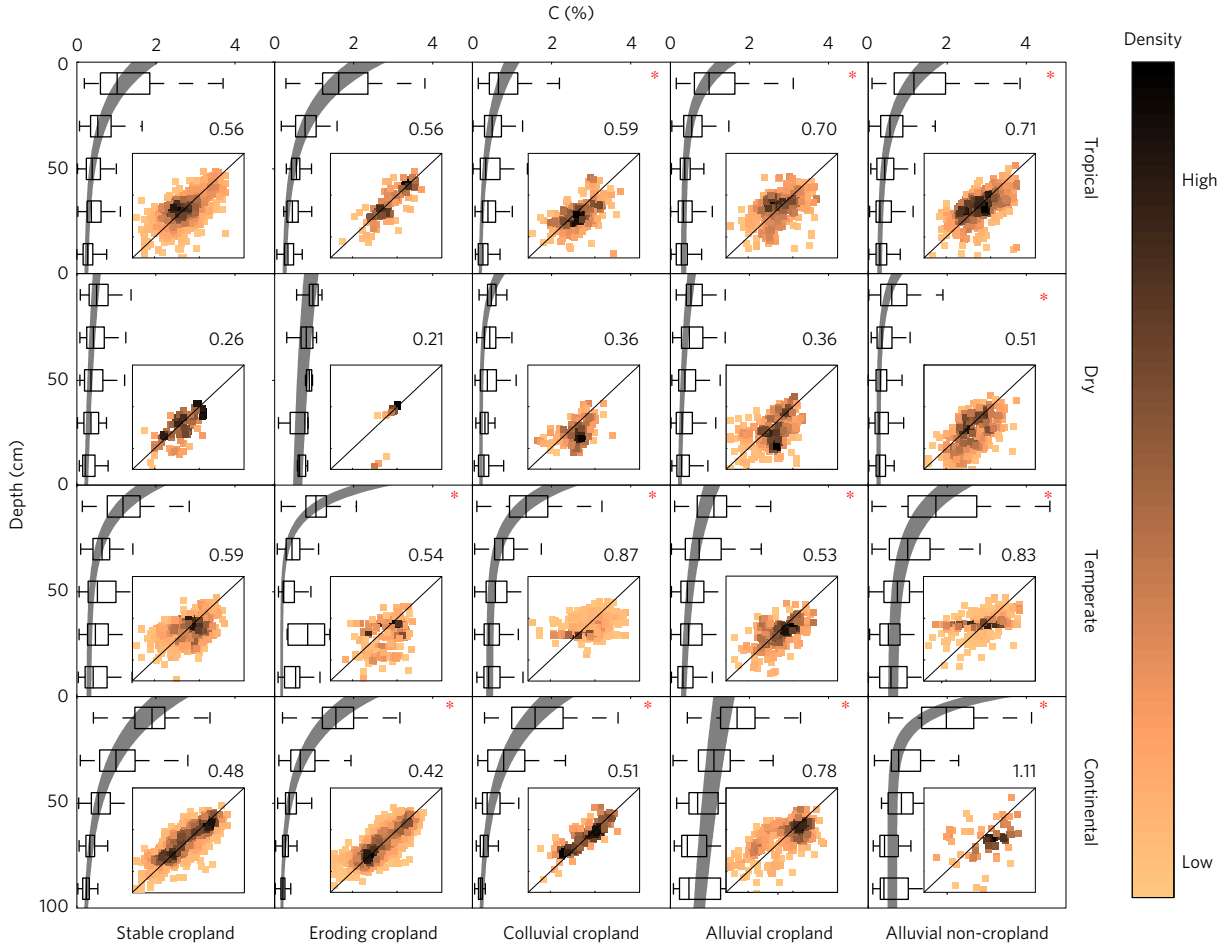

Figure 3 | Observed and simulated SOC profiles for 20 climate–geomorphic classes. The box plots represent the distribution (5th, 25th, 50th, 75th and 95th percentiles) of the observed SOC content for different depth layers (0–20 cm, 20–40 cm, 40–60 cm, 60–80 cm and 80–100 cm). The grey zones represent the uncertainty ranges for the average SOC profiles that were used in the model simulations. These ranges correspond to the coefficients reported in Supplementary Table 2 and the C scaling factor in Supplementary Table 4. 70% of the observations were used for model calibration while the remaining 30% were used for validation. Figure insets present a scatterplot of observed (*x* axis) versus predicted (*y* axis) SOC contents (%C, log scale) for the validation data. Numbers in the plots present the validation RMSE (%C) of each climate–geomorphic class. An asterisk denotes that the coefficients of the corresponding nonlinear regression are significantly different from those of the stable site within the same climate zone (sum of square reduction test, $P < 0.05$).

same period. This suggests that C stabilization in newly exposed subsoil results in efficient SOC recovery. Although our data contain cases where erosion-induced ecosystem degradation resulted in substantial SOC decline, at the global scale, erosional SOC loss is predominantly maintained over long timescales. This is consistent with both empirical and model-based observations and is probably related to the fact that only a small fraction of NPP, typically less than 10%, is removed by erosion, even at higher erosion rates[21,22].

A large fraction of C mobilized by agricultural erosion is redeposited in colluvial and alluvial soils; we estimated a global C influx of 357 ± 136 (colluvia) and 243 ± 84 (alluvia) Pg to these stores, respectively. The mobilized SOC can be exposed to accelerated decomposition during transport[23,24] while deposited SOC can be efficiently protected from decomposition in low mineralization contexts, leading to C sinks in colluvial and alluvial sediments[25–28]. The amount of C buried and stored in these environments depends on the nature and amount of mobilized C, the C lost during transport, the rate of C burial, and the postdepositional environmental conditions[20,26]. We estimated that SOC stocks in colluvial and alluvial soils increased by only 58 ± 17 and 30 ± 10 Pg C, respectively. This implies high rates of postdepositional losses and a relatively low C burial efficiency of only 15–19%. These global estimates are on the same order of magnitude, but lower than previously reported burial efficiencies for colluvial and alluvial stores, which range between 20–30% (refs 25,27,28) and 25–100% (refs 27–29), respectively.

The efficient stabilization of SOC at the sites of erosion[18], together with the burial and partial preservation of both allochthonous and autochthonous C in depositional environments[26–28] observed here, provides a mechanism for erosion-induced net C uptake on land[30]. Our simulations show that when averaged over the period of agriculture, one unit of laterally transported SOC caused 0.21–0.28 units of C to be sequestered from the atmosphere into the terrestrial biosphere. Past agricultural soil erosion has thus resulted in a C uptake on land (ΔVC_l) of 191 ± 62 Pg (Fig. 1). We estimated that agricultural erosion has resulted in a flux of 159 ± 56 Pg from land to aquatic systems. This flux (C_{ex}), whose magnitude is comparable to that of ΔVC_l, is thus significant for the overall C budget. Rivers do not passively transport terrestrial organic C, but act as a C source for the atmosphere through the metabolism of this C[31,32]. We estimated a cumulative C flux from rivers to the atmosphere of 15 ± 7 Pg. Meanwhile, a fraction of the eroded terrestrial C is transported to lakes or eventually the ocean. The C burial efficiencies reported in the literature for these environments are substantially larger than those obtained here for colluvial and alluvial soils (that is, 22–60% versus 15–19%). Nevertheless, a substantial fraction of the terrestrial particulate organic C (POC)

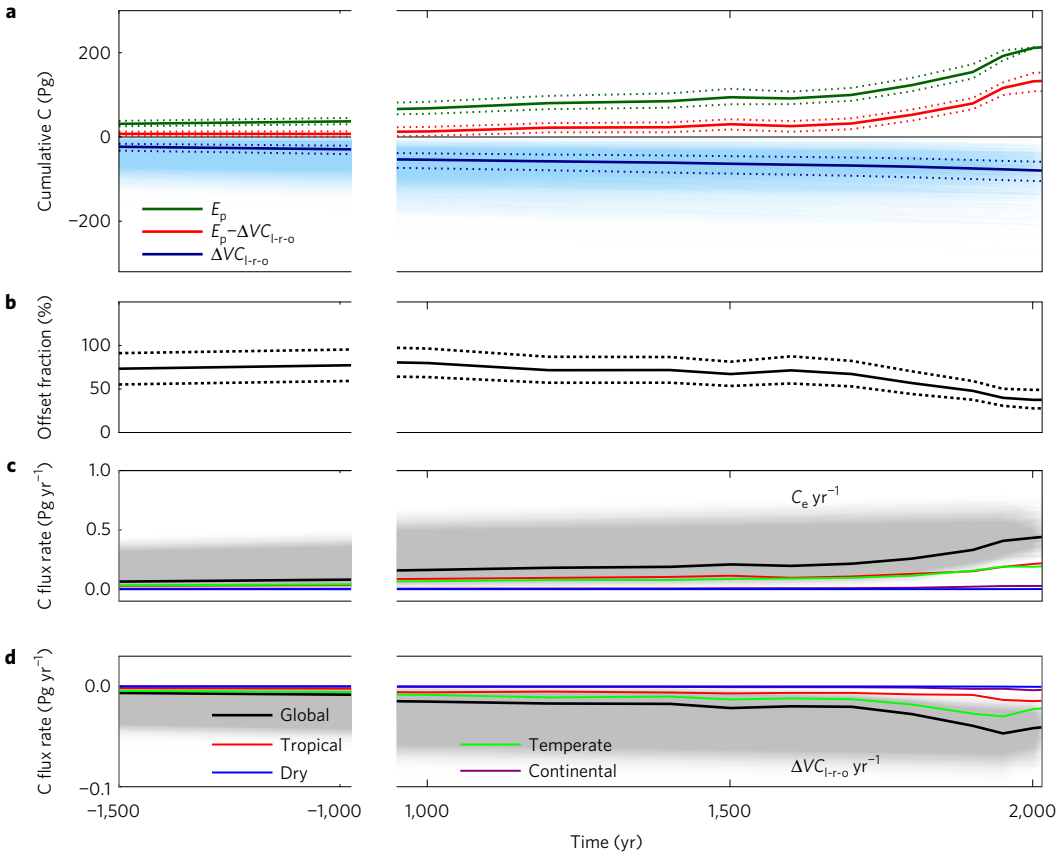

Figure 4 | Temporal evolution of land–atmosphere C fluxes due to primary ALCC emissions and erosion/burial. a, Cumulative C emissions resulting from the direct effect of ALCC, that is, the C release due to a reduction in vegetation and soil C (E_p), cumulative C uptake resulting from the indirect effect of ALCC through agricultural erosion and burial of SOC ($\Delta VC_{l\text{-}r\text{-}o}$) and the net balance ($E_p$-$\Delta VC_{l\text{-}r\text{-}o}$). Negative values denote a flux towards the land; positive values denote a flux towards the atmosphere. The blue shading around $\Delta VC_{l\text{-}r\text{-}o}$ represents the result of individual model scenarios (a total of 10,000 scenarios were considered). **b**, The offset fraction of erosion-induced C sink ($\Delta VC_{l\text{-}r\text{-}o}$) to the primary emission by ALCC (E_p). In **a** and **b**, solid lines represent the median model simulation while the dotted lines represent the 25th and 75th percentiles. **c**,**d**, The temporal evolution of SOC mobilization (C_e yr^{-1}) and erosion-induced vertical C flux of the land–river–ocean system ($\Delta VC_{l\text{-}r\text{-}o}$ yr^{-1}) per climate zone. The grey shading represents the result of individual model scenarios at the global scale.

entering aquatic systems is mineralized before being stabilized in lake and continental margin sediments[6,33]. We estimated that 96 ± 34 Pg of terrestrial OC was mineralized in lakes and oceans, while 47 ± 16 Pg was stabilized in sediments. CH_4 emissions from the aquatic systems due to the mineralization of POC resulted in an additional flux of 1.1 ± 0.43 Pg C (7.2 ± 2.8 Pg C-CO_2 equivalent). When considering the overall C balance between atmospheric loss terms and accumulation in sediments across the geomorphic cascade, agricultural erosion has induced a net uptake of 78 ± 22 Pg C into the land–river–ocean system ($\Delta VC_{l\text{-}r\text{-}o}$) during the whole agricultural period (Figs 1 and 4a). The tropical and temperate climate zones accounted for about 96% of this C uptake. This contribution is disproportionately large considering their share of global cropland area (about 59%), which implies that these climate zones are more efficient in terms of the erosion-induced C uptake than the dry and continental climate zones (Fig. 4d). The underlying factors controlling this are related to higher precipitation that results in higher NPP, C input and stocks as well as more energy to mobilize and transport soil particles. Although the pre-industrial period accounts for a large part of this net cumulative uptake of C, annual flux rates have increased by a factor of 4.6 since AD 1850.

Our estimates of C cycle perturbations resulting from agricultural erosion and burial help to constrain mechanisms that influenced the past C cycle. On the basis of the existing literature, we estimated that ALCC has resulted in cumulative emissions of 139 ± 16 Pg C for the pre-industrial era (Fig. 4a), considering only direct effects (that is, reduction in vegetation and soil C, see Supplementary Methods 1 Section 3). However, our results show that current scenarios of pre-industrial C emissions may not accurately represent the net anthropogenic C flux between land and atmosphere, because the acceleration of erosion associated with ALCC results in a substantial C sink that has hitherto been neglected. Our estimates of the pre-industrial net erosion-induced C uptake for the land–river–ocean system represent 51 ± 12% of the ALCC-induced direct C loss from vegetation and soils (Fig. 4b). Given that erosion processes are omitted from existing analyses, current scenarios may substantially overestimate past terrestrial C losses. Isotopic data have shown that long-term C emissions from ALCC must have been greatly offset by a large and hitherto unidentified terrestrial C sink[11]. On the basis of our analysis, we argue that agricultural erosion and burial processes are a substantial proportion of this unidentified sink because our estimates go a long way towards reconciling the differences between modelled anthropogenic emissions and observed atmospheric CO_2 concentrations[11]. Furthermore, studies have reported a strong and continuous buffering of primary ALCC emissions by the biosphere, whereby less than 50% has remained airborne[3]. Our results strongly suggest that assessments omitting erosion from ALCC forcing scenarios may lead to biased interpretations of the past and current biosphere–atmosphere coupling, because primary ALCC emissions are to a large extent compensated for by the erosion-induced C sink.

Our simulations are in good agreement with previously estimated erosion-induced sediment and C fluxes (see Supplementary Methods 2). It should be noted that we considered only cropland in our analysis, while other practices such as overgrazing in marginal zones may also lead to accelerated erosion[10]. On the basis of a sensitivity analysis (see Supplementary Methods 1), we identified the ALCC reconstruction and SOC mobilization as the largest sources of uncertainty for our estimates of erosion-induced C fluxes in the pre-industrial era (Supplementary Fig. 8a). This contrasts with the industrial period, where the ALCC scenario reconstruction is much better constrained and land surface connectivity, which controls whether C is buried in soils or aquatic sediments, becomes one of the key controls on the C cycle (Supplementary Fig. 8b). Furthermore, our estimations show that up to about AD 1600, erosion-induced uptake offset 70 ± 16% of C emission by ALCC, whereas after AD 1600, ALCC emissions began to increase more rapidly, resulting in a smaller cumulative offset of 37 ± 10% at present (2015) (Fig. 4b). This reflects the rapid release of biomass C to the atmosphere after ALCC. In contrast, the erosional sink operates at a much slower pace, but has a much longer duration (Fig. 4a). The magnitude and temporal variability of C erosion and the associated C sink also imply that a more detailed assessment of the spatial and temporal variability of C erosion and burial processes is required to fully understand the relative importance of natural climate variability versus human-induced climate change over the last millennia and to improve our capacity to predict changes in land C as a result of future land cover and climate change. We emphasize the need for erosion control for the benefits it brings for soil quality and the delivery of ecosystem services. However, with erosion exacerbated by climatic extremes and a sharp increase in global food demand[34], we argue that not accounting for erosion-induced C fluxes may result in biased estimates of the carbon budget.

Methods

Methods, including statements of data availability and any associated accession codes and references, are available in the online version of this paper.

Received 27 February 2016; accepted 9 March 2017; published online 10 April 2017

References

1. Houghton, R. A. *et al*. Carbon emissions from land use and land-cover change. *Biogeosciences* **9,** 5125–5142 (2012).
2. Kaplan, J. O. *et al*. Holocene carbon emissions as a result of anthropogenic land cover change. *Holocene* **21,** 775–791 (2011).
3. Pongratz, J., Reick, C. H., Raddatz, T. & Claussen, M. Effects of anthropogenic land cover change on the carbon cycle of the last millennium. *Glob. Biogeochem. Cycles* **23,** GB4001 (2009).
4. Berner, R. A., Lasaga, A. C. & Garrels, R. M. The carbonate-silicate geochemical cycle and its effect on atmospheric carbon dioxide over the past 100 million years. *Am. J. Sci.* **283,** 641–683 (1983).
5. Gaillardet, J., Dupré, B., Louvat, P. & Allègre, C. J. Global silicate weathering and CO_2 consumption rates deduced from the chemistry of large rivers. *Chem. Geol.* **159,** 3–30 (1999).
6. Burdige, D. J. Burial of terrestrial organic matter in marine sediments: a re-assessment. *Glob. Biogeochem. Cycles* **19,** GB4011 (2005).
7. Galy, V. *et al*. Efficient organic carbon burial in the Bengal fan sustained by the Himalayan erosional system. *Nature* **450,** 407–410 (2007).
8. Galy, V., Peucker-Ehrenbrink, B. & Eglinton, T. Global carbon export from the terrestrial biosphere controlled by erosion. *Nature* **521,** 204–207 (2015).
9. Montgomery, D. R. Soil erosion and agricultural sustainability. *Proc. Natl Acad. Sci. USA* **104,** 13268–13272 (2007).
10. Cerdan, O. *et al*. Rates and spatial variations of soil erosion in Europe: a study based on erosion plot data. *Geomorphology* **122,** 167–177 (2010).
11. Bauska, T. K. *et al*. Links between atmospheric carbon dioxide, the land carbon reservoir and climate over the past millennium. *Nat. Geosci.* **8,** 383–387 (2015).
12. Chappell, A., Baldock, J. & Sanderman, J. The global significance of omitting soil erosion from soil organic carbon cycling schemes. *Nat. Clim. Change* **6,** 187–191 (2016).
13. Quinton, J. N., Govers, G., Van Oost, K. & Bardgett, R. D. The impact of agricultural soil erosion on biogeochemical cycling. *Nat. Geosci.* **3,** 311–314 (2010).
14. Van Oost, K. *et al*. The impact of agricultural soil erosion on the global carbon cycle. *Science* **318,** 626–629 (2007).
15. Quine, T. A. & Van Oost, K. Quantifying carbon sequestration as a result of soil erosion and deposition: retrospective assessment using caesium-137 and carbon inventories. *Glob. Change Biol.* **13,** 2610–2625 (2007).
16. Lal, R. Soil erosion and the global carbon budget. *Environ. Int.* **29,** 437–450 (2003).
17. Berhe, A. A., Harte, J., Harden, J. W. & Torn, M. S. The significance of the erosion-induced terrestrial carbon sink. *Bioscience* **57,** 337–346 (2007).
18. Harden, J. W. *et al*. Dynamic replacement and loss of soil carbon on eroding cropland. *Glob. Biogeochem. Cycles* **13,** 885–901 (1999).
19. Bakker, M., Govers, G., Jones, R. & Rounsevell, M. A. The effect of soil erosion on Europe's crop yields. *Ecosystems* **10,** 1209–1219 (2007).
20. Berhe, A. A., Harden, J. W., Torn, M. S. & Harte, J. Linking soil organic matter dynamics and erosion-induced terrestrial carbon sequestration at different landform positions. *J. Geophys. Res.* **113,** G04039 (2008).
21. Li, Y. *et al*. Sustained high magnitude erosional forcing generates an organic carbon sink: test and implications in the Loess Plateau, China. *Earth Planet. Sci. Lett.* **411,** 281–289 (2015).
22. Smith, S. V. *et al*. Soil erosion and significance for carbon fluxes in a mountainous Mediterranean-climate watershed. *Ecol. Appl.* **17,** 1379–1387 (2007).
23. Van Hemelryck, H., Fiener, P., Van Oost, K., Govers, G. & Merckx, R. The effect of soil redistribution on soil organic carbon: an experimental study. *Biogeosciences* **7,** 3971–3986 (2010).
24. Jacinthe, P. A., Lal, R., Owens, L. B. & Hothem, D. L. Transport of labile carbon in runoff as affected by land use and rainfall characteristics. *Soil Tillage Res.* **77,** 111–123 (2004).
25. Wang, Z. *et al*. The fate of buried organic carbon in colluvial soils: a long-term perspective. *Biogeosciences* **11,** 873–883 (2014).
26. Wang, Z., Van Oost, K. & Govers, G. Predicting the long-term fate of buried organic carbon in colluvial soils. *Glob. Biogeochem. Cycles* **29,** 65–79 (2015).
27. Van Oost, K. *et al*. Legacy of human-induced C erosion and burial on soil–atmosphere C exchange. *Proc. Natl Acad. Sci. USA* **109,** 19492–19497 (2012).
28. Hoffmann, T., Schlummer, M., Notebaert, B., Verstraeten, G. & Korup, O. Carbon burial in soil sediments from Holocene agricultural erosion, Central Europe. *Glob. Biogeochem. Cycles* **27,** 828–835 (2013).
29. Omengo, F. O., Geeraert, N., Bouillon, S. & Govers, G. Deposition and fate of organic carbon in floodplains along a tropical semiarid lowland river (Tana River, Kenya). *J. Geophys. Res.* **121,** 1131–1143 (2016).
30. Stallard, R. F. Terrestrial sedimentation and the carbon cycle: coupling weathering and erosion to carbon burial. *Global Biogeochem. Cycles* **12,** 231–257 (1998).
31. Aufdenkampe, A. K. *et al*. Riverine coupling of biogeochemical cycles between land, oceans, and atmosphere. *Front. Ecol. Environ.* **9,** 53–60 (2011).
32. Raymond, P. A. *et al*. Global carbon dioxide emissions from inland waters. *Nature* **503,** 355–359 (2013).
33. Blair, N. E. & Aller, R. C. The fate of terrestrial organic carbon in the marine environment. *Ann. Rev. Mar. Sci.* **4,** 401–423 (2012).
34. Tilman, D., Balzer, C., Hill, J. & Befort, B. L. Global food demand and the sustainable intensification of agriculture. *Proc. Natl Acad. Sci. USA* **108,** 20260–20264 (2011).

Acknowledgements

Z.W. is funded by BELSPO (IUAP programme, contract: P7-24). J.O.K. is supported by the European Research Council (313797 COEVOLVE). K.V.O. is a Senior Research Associate of the Fonds de la Recherche Scientifique (FNRS), Belgium. Support for this project was provided by the FNRS (convention number 2.4590.12). We thank S. Bouillon, H. Maclean, T. A. Quine and A. Stevens for comments on earlier versions of the manuscript.

Author contributions

Z.W. and K.V.O. conceived the research; Z.W. performed the analysis; Z.W. and K.V.O. co-wrote the paper. All authors assisted in the interpretation of the results and commented on the manuscript.

Additional information

Supplementary information is available in the online version of the paper. Reprints and permissions information is available online at www.nature.com/reprints. Publisher's note: Springer Nature remains neutral with regard to jurisdictional claims in published maps and institutional affiliations. Correspondence and requests for materials should be addressed to Z.W.

Competing financial interests

The authors declare no competing financial interests.

Methods

Global soil profile database analysis. Soil profile data (19,816 observations) from different sources were compiled to analyse SOC profiles for 20 climate–geomorphic combinations. For soil profiles in each climate zone, information related to land use, soil type, parent material, slope gradient, landform and slope position was used to classify the soil profiles into five groups (stable cropland, eroding cropland, colluvial cropland, alluvial cropland and alluvial non-cropland). Given that soil texture and depth are important factors controlling SOC content[35–37], 'type' SOC profiles for the 20 climate–geomorphic combinations were modelled using nonlinear regression:

$$C(z) = \mathrm{Clay}(z) \times (\alpha \times e^{(-\beta \times z)} + \gamma) \quad (1)$$

where C(z) (%) is the C content at depth z (m), Clay(z) (%) is the clay content at depth z (m), z is the soil depth (m), and α, β and γ are coefficients. The results of the regression analysis are presented in Supplementary Table 2 and Fig. 3. Note that the uncertainty surrounding these 'type' profiles is explicitly accounted for in our model scenarios (see Supplementary Methods 3 Equation 19).

Model approach. Agricultural erosion was simulated using a model based on land use, climate and relief[14]. The model was validated using the results of the National Resource Inventory (NRI) for the US[38] and a large experimental database for Europe[10]. Only water erosion on cropland, which is by far the dominant human-induced erosion process[14], was considered in this study. Driven by the spatial and temporal evolution of agricultural land use (based on HYDE[39,40] and KK10[41] anthropogenic land use scenarios) and a validated soil erosion model (see above), the model simulates the transfer of sediment and SOC between five geomorphic units within, as well as the sediment and SOC export from, each catchment. Changes in SOC stock, relative to a non-eroding cropland profile, reflect the combined effect of lateral C fluxes (that is, lateral C input or loss) and erosion-induced soil–atmosphere C exchange[15,27]. Details on the model components and equations are provided in the Supplementary Methods.

Model implementation. The model was implemented using 1,000 virtual catchments in four climatic zones. To assess erosion-induced C fluxes, we explored an entire range of possible model parameter sets by modelling agricultural erosion as a series of 10,000 scenarios. The ranges of the model parameters are presented in Supplementary Table 4. The probability distribution of the model scenarios was estimated using the generalized likelihood uncertainty estimation (GLUE) approach by confronting the simulated cumulative sediment flux with data from 13 catchments, covering a large variety of agricultural trajectories and environmental conditions (Supplementary Fig. 2).

Data availability. The map of climate zones is available at the website of Köppen–Geiger climate classification (http://koeppen-geiger.vu-wien.ac.at/present.htm). HYDE land use data are available at the website of History Database of the Global Environment from Netherlands Environmental Assessment Agency (http://themasites.pbl.nl/tridion/en/themasites/hyde/download/index-2.html). The Gridded Soil Survey Geographic (gSSURGO) Database is available at the website of United States Department of Agriculture (http://www.nrcs.usda.gov/wps/portal/nrcs/detail/soils/survey/geo/?cid=nrcs142p2_053628). The US Soil Characterization Database of National Cooperative Soil Survey (NCSS) is available at the website of United States Department of Agriculture (http://www.nrcs.usda.gov/wps/portal/nrcs/main/soils/survey/tools). The Brazil soil database is available for free download at http://www.esalq.usp.br/gerd. The WISE-Global World Soil Profile Database (v.3.1) is available at the website of ISRIC (http://www.isric.org/data/isric-wise-global-soil-profile-data-ver-31). The Africa Soil Profiles Database (AfSP) is available at the website of ISRIC (http://www.isric.org/content/africa-soil-profiles-database-afsp). Other data that support the findings of this study are available from the corresponding author on request.

References

35. Zinn, Y. L., Lal, R., Bigham, J. M. & Resck, D. V. S. Edaphic controls on soil organic carbon retention in the Brazilian Cerrado: Texture and mineralogy. *Soil Sci. Soc. Am. J.* **71,** 1204–1214 (2007).
36. Jobbágy, E. G. & Jackson, R. B. The vertical distribution of soil organic carbon and its relation to climate and vegetation. *Ecol. Appl.* **10,** 423–436 (2000).
37. Feller, C. & Beare, M. H. Physical control of soil organic matter dynamics in the tropics. *Geoderma* **79,** 69–116 (1997).
38. *2007 National Resources Inventory* Summary Report (Natural Resources Conservation Service, Center for Survey Statistics and Methodology, 2009).
39. Klein Goldewijk, K., Beusen, A., van Drecht, G. & de Vos, M. The HYDE 3.1 spatially explicit database of human-induced global land-use change over the past 12,000 years. *Glob. Ecol. Biogeogr.* **20,** 73–86 (2011).
40. Klein Goldewijk, K., Beusen, A. & Janssen, P. Long-term dynamic modeling of global population and built-up area in a spatially explicit way: HYDE 3.1. *Holocene* **20,** 565–573 (2010).
41. Kaplan, J. O., Krumhardt, K. M. & Zimmermann, N. The prehistoric and preindustrial deforestation of Europe. *Quat. Sci. Rev.* **28,** 3016–3034 (2009).